Implication of polymeric template agent on the formation process of hybrid halide perovskite film

Implication of polymeric template agent on the formation process of hybrid halide perovskite film

To cite this article before publication: Antonella Giuri *et al* 2021 *Nanotechnology* in press https://doi.org/10.1088/1361-6528/abed72

IOP Publishing Journal Title
Journal **XX** (XXXX) XXXXXX https://doi.org/XXXX/XXXX

Implication of polymeric template agent on the formation process of hybrid halide perovskite film

Antonella Giuri[1], Rahim Munir[2,3], Andrea Listorti[1,4], Carola Esposito Corcione[1,5], Giuseppe Gigli[1,6], Aurora Rizzo[1], Aram Amassian[2*] and Silvia Colella[7*]

[1] Istituto di Nanotecnologia CNR-Nanotec, Polo di Nanotecnologia c/o Campus Ecotekne Via Monteroni, 73100 Lecce, Italy
[2] King Abdullah University of Science and Technology (KAUST) Physical Sciences and Engineering Division (PSE), and KAUST Solar Center (KSC) Thuwal 23955-6900, Saudi Arabia
[3] Department of Chemistry, University of Calgary, 2500 University Drive N.W., Calgary, Alberta, T2N 1N4, Canada
[4] Department of Chemistry, University of Bari "Aldo Moro", via Orabona 4, 70126 Bari, Italy
[5] Dipartimento di Ingegneria dell'Innovazione, Università del Salento, via per Monteroni, km 1,73100, Lecce, Italy
[6] Dipartimento di Matematica e Fisica, Università del Salento, via per Monteroni, km 1,73100, Lecce, Italy
[7] Istituto di Nanotecnologia CNR-Nanotec, c/o Dipartimento di Chimica, Università di Bari, Via Orabona 4, Bari, Italy

E-mail: silvia.colella@nanotec.cnr.it

Received xxxxxx
Accepted for publication xxxxxx
Published xxxxxx

Abstract

The use of polymeric additives supporting the growth of hybrid halide perovskites has proven to be a successful approach aiming at high quality active layers targeting optoelectronic exploitation. A detailed description of the complex process involving the self-assembly of the precursors into the perovskite crystallites in presence of the polymer is, however, still missing. Here we take starch:$CH_3NH_3PbI_3$ ($MAPbI_3$) as example of highly performing composite, both in solar cells and light emitting diodes, and study the film formation process through differential scanning calorimetry and in situ time-resolved grazing incidence wide-angle X-ray scattering, performed during spin coating. These measurements reveal that starch beneficially influences the nucleation and growth of the perovskite precursor phase, leading to improved structural properties of the resulting film which turns into higher stability towards environmental conditions.

Keywords: starch:$MAPbI_3$ composite, perovskite crystallisation, differential scanning calorimetry (DSC), Grazing-incidence wide-angle X-ray scattering (GIWAX)

1. Introduction

Hybrid halide perovskites have revolutionized the field of optoelectronic with the promise to bring to the market a low-cost, high-efficient, and versatile thin-film technology.

Thanks to the eclectic features of hybrid perovskites [1], various kind of optoelectronic devices have so far been explored with great success, mainly solar cells [2–4] and light emitting diodes (LEDs) [2,5,6]. Perovskites are formed from solution by self-assembly of precursors and have been deposited on a plethora of substrates; in fact, various device layouts have been proposed so far, with special emphasis on the design and processing of polycrystalline perovskite into a planar device architecture. Thereby, much effort has been focused in improving the surface coverage of the solution-processed perovskite active layer and making the deposition process easily scalable and robust [7].

Nowadays different approaches exist to control the growth of perovskite films, specifically acting on the morphology, crystallinity and moisture resistance, spanning from thermal treatments, additive inclusion, variations on the precursors stoichiometry. [5,8–15] In combination with these strategies, the use of antisolvent dripping during the deposition of perovskite precursors is largely exploited to obtain better film morphology and properties [16,17]. However, such method is hardly compatible with large-scale production, where the simple deposition in one-step coating is clearly more suitable. One of the most attractive approaches in this sense is the use of polymeric templating agents to grow, via single step processing, perovskite films, as it has shown to improve the stability of the perovskite material and to make its deposition more facile and compatible with large-scale manufacturing [9,18].

We recently demonstrated how the addition of starch as rheological modifier in the perovskite precursor solution enables the deposition of a thick and continuous perovskite film with a simple single spin-coating step, allowing to eliminate the solvent dripping step, which generally employs toxic solvents. [19]. The presence of starch allows to conveniently mold the polycrystalline layer leading to a material that presents improved morphology and high resistance to moisture, with obvious positive implications on the processing of the whole device [5,20]. In fact, with this straightforward approach, we obtained improved efficiency and stability of photovoltaic devices [20], as well as ultra-bright LEDs [5] with reduced efficiency roll-off. Concerning LEDs, the use of starch allowed to modulate the growth of perovskite micro/nano-structures and to physically confine the α-δ formamidinium lead iodide ($FAPbI_3$) perovskite mixed phase, eventually acting as a charge carrier concentrators to favour radiative recombination and to reduce efficiency roll-off at high current density.

The stability of the developed perovskite-starch nanocomposite was analyzed in our previous work by placing the films and the respective photovoltaic devices without encapsulation in ambient air (temperature ~22 °C, moisture content 40-70%) [20]. The retention of 36% of initial PCE after 816 h of aging test can be attributed to the beneficial protection effect of the hygroscopic starch from ambient environment contamination (in particular oxygen and moisture), but it can surely be related also to a difference in the perovskite crystalline domains that are induced by the presence of starch, likely due to a change in the formation process.

To explore the effect of starch modifier on the perovskite crystallization herein we investigate the formation process of perovskite films through a double approach using Differential Scanning Calorimetry (DSC) and in situ Grazing-incidence wide-angle X-ray scattering (GIWAX) performed during spin coating. GIWAXS has emerged as a powerful tool to study the micro-structural evolution of perovskites from the precursors solution to the solid state, shining light on the formation process of crystalline intermediates and byproducts [21,22]; DSC, on the other side, represents a much more simple and straightforward technique to determine the kinetic of solidification and collecting information on the thermodynamic evolution of the reaction. Thanks to this complementary approach, we show that starch forms within the precursor solutions a sol-gel network that is stabilized thanks to specific interactions with the precursor solvate phase and the increase of media viscosity. This network impacts the polycrystalline film formation of the hybrid perovskite, thanks to a delayed collapse of this disordered sol-gel phase into the crystalline products leading to more crystalline and thermodynamically stable perovskite domains.

Experimental Section

Materials

Lead (II) iodide (PbI2, ultradry 99.999% metals basis) and methylammonium iodide CH_3NH_3I (MAI) was purchased from Alfa Aesar and Dyesol, respectively. Dimethyl sulfoxide anhydrous, 99.9% (DMSO) was purchased from Aldrich. Corn starch (Maizena) was supplied from Unilever.

$MAPbI_3$:starch based solution preparation

The perovskite used was prepared by following the method developed in our previous work [20]. In details, equimolar stoichiometry perovskite precursors (MAI: PbI_2 = 1:1) were solubilized in DMSO, at 80 °C for 30 min, with precursors concentration of 30 wt%. Subsequently, 5-10 and 15 wt% of

starch amounts were added to perovskite precursors (for 30MAPbI$_3$-5S, 30MAPbI$_3$-10S, 30MAPbI$_3$-15S, respectively), followed by stirring at 80 °C for 5 h. All the solutions were prepared in N_2 filled glove-box.

Films deposition

Glass ITO coated substrates (Visiontek Systems Ltd.) were sequentially cleaned by ultrasonication in acetone and deionized water. Perovskite:starch nanocomposite film was obtained by spin coating the solution at 6000 rpm for 20 s and annealed at 100º C for 30 min.

Characterization

GIWAX. The in situ GIWAXS experiments were conducted in ambient environment (R.H. ≈ 20%) at D1 beam line at the Cornell High Energy Synchrotron Source following the protocol described in ref. [23,24]. A custom-built spin coater was used for precursors solution spin coating. The detector used was a Pilatus 200K area detector.

Differential Scanning Calorimetry (DSC). Dynamic DSC scans were performed on starch-perovskite precursor solutions by a differential scanning calorimeter (DSC Mettler Toledo 622). The crucibles were prepared by dropping about 3 µL of each solution into a sealed pan with a perforated lid, in order to allow the evaporation of solvents and by-product. The samples were heated from 25 up to 250 °C at 10 °C/min scan rate under nitrogen flow (80 ml/min). Three measurements were performed on each sample. The crystallization enthalpy, Hc, was deduced from the area of the respective exotherms based on an extrapolated horizontal baseline aligned to the asymptotic value of the DSC signal at the end of the reaction. The onset temperature, T_{onset}, was calculated by extrapolating the intersection point between the tangent lines to the curve at the beginning of the reaction.

Thermogravimetric analysis (TGA). Dynamic TGA were performed on starch-perovskite precursor solutions by a TA Instrument SDT Q600. The crucible were prepared by dropping about 6µL of each solutions into an alumina pan sealed with a perforated lid. All was heated from 20 to 700 °C under nitrogen atmosphere (100 ml/min) at a heating rate of 10 °C/min. Three measurements were performed on each sample. The onset temperature, T_{onset}, was calculated by extrapolating the intersection point between the tangent lines to the curve at the beginning of the weight loss.

Results and discussion

DSC dynamic measurements were performed on the formulation containing 30 wt% of perovskite precursors, with 5-10-15 wt% of starch (30MAPbI$_3$-5S, 30MAPbI$_3$-10S-30MAPbI$_3$-15S, respectively) and without starch (30MAPbI$_3$). The aim of this analysis is to study the effect of starch on the thermal behaviour of the perovskite and to measure the crystallization enthalphy, closely related to the thermodynamic stability of the final product. DSC thermograms acquired are shown in Figure 1 (a) and (b).

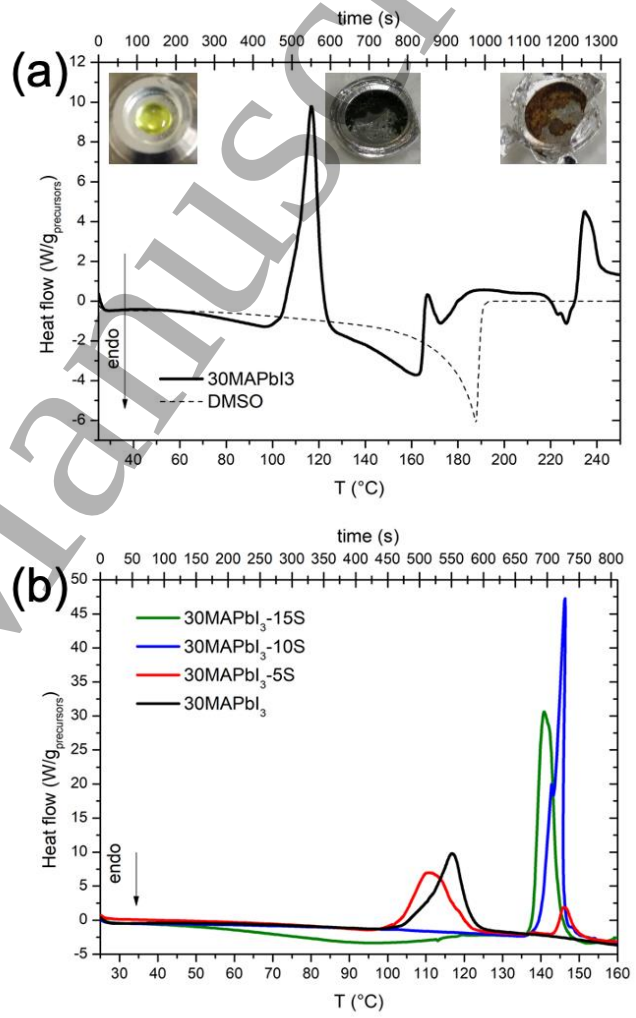

Figure 1. DSC heating thermograms up to 250 °C measured at 10 °C/min for DMSO and 30MAPbI3, with the evolution of the perovskite precursors solution in the pan during the measurement showed in the inset (a), comparison between the perovskite precursors solutions DSC thermograms up to 160 °C, and the composites containing starch (b)

Table 1. Noticeable DSC values of perovskite precursors solutions with increasing starch content (average values with standard deviation calculated for three measurements)

Sample	ΔH_c J/g	Peak 1		Peak 2	
		T_{onset} °C	T_{peak} °C	T_{onset} °C	T_{peak} °C
30MAPbI$_3$	630.6 ± 16.2	100.9 ± 11.4	109.5 ± 10.3		
30MAPbI$_3$-5S	755.1 ± 16.8	103.6 ± 1.3	110.6 ± 0.4	143.9 ± 0.2	146.9 ± 0.8
30MAPbI$_3$-10S	870.7 ± 7.9			145.4 ± 3.7	149.7 ± 4.5
30MAPbI$_3$-15S	952.8 ± 26.9			143.1 ± 5.1	148.1 ± 5.6

By comparing the DSC data collected for the perovskite precursors solution with DMSO curve, it is evident that the thermograms endowed the overlapping of the two opposite phenomena: solvent evaporation (endothermic) and perovskite crystallization (exothermic) occurring during the measurement, evidencing the presence of clear and intense exothermic peak associated to the perovskite formation. As showed in figure 1(a) and quantitatively reported in table 1, the pristine 30MAPbI$_3$ sample presents an exothermic peak at 109.5 ± 10.3 °C, with an onset at 100.9 ± 11.4 °C, associated to the crystallization process, as also confirmed by the modification of the sample from yellow liquid to dark solid (inset figure 1(a)). Moreover, the exothermic peaks at temperature higher than 160 °C are related to degradation processes that occur into the sample, as also evidenced by the inset in figure 1(a). It is interesting to note that along with the first peak at 110.6 ± 0.4 °C, a second exothermic peak at higher temperature (146.9 ± 0.8 °C) appears after adding 5 wt% of starch (figure 1(b)), that completely replaces the first one for higher starch concentrations: in fact the crystallization occurs at 149.7 ± 4.5 °C for 30MAPbI$_3$-10S and 148.1 ± 5.6 °C for 30MAPbI$_3$-15S. The temperature onset for both of them is estimated around 145 °C. Deducing the crystallization enthalpy ΔHc from the area of the respective exotherms in Figure 1(b) we found that this is also affected by the presence of starch. In fact, ΔH_c increases from a value of 630.6 ± 16.2 J/g for the pristine sample to 755.1 ± 16.8, 870.7 ± 7.9, and 952.8 ± 26.9 J/g for the 30MAPbI$_3$-5S, 30MAPbI$_3$-10S, 30MAPbI$_3$-15S respectively (Table 1). These evidences suggest that the addition of starch in the perovskite solution can interfere with multiple processes: firstly with the evaporation of DMSO solvent, that requires a higher energy in the presence of starch due to the existence of specific interactions polymer-solvent, as further corroborated by Thermogravimetric Analysis (TGA) measuring the weight loss of the different solutions with temperature, shown in Figure 2. In particular, the onset temperature of the first weight loss step, associated to the evaporation of DMSO, is reported in the table (Figure 2) for all the precursor solutions and shows a change in the evaporation temperature from about 100 °C (for 30MAPbI$_3$) to about 119°C in the presence of increasing amounts of starch.

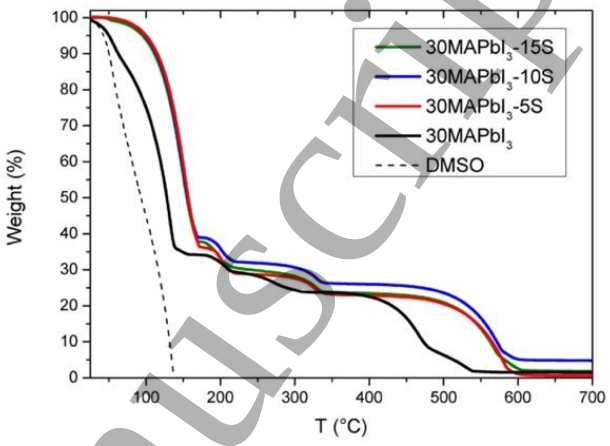

Sample	DMSO evaporation
	T_{onset} °C
30MAPbI$_3$	100.4 ± 0.1
30MAPbI$_3$-5S	119.6 ± 2.5
30MAPbI$_3$-10S	118.7 ± 2.0
30MAPbI$_3$-15S	118.5 ± 2.8

Figure 2. TGA heating thermograms up to 700 °C measured at 10 °C/min for DMSO and 30MAPbI$_3$ precursor solutions containing different starch concentration, with onset temperature values related to DMSO evaporation in the table. (Average values with standard deviation calculated for three measurements)

On the other hand, starch interferes with the nucleation and assembly process through gel-network formation, with a stronger influence as the starch concentration increases (in the investigated range). In addition, a higher enthalpy measured for the perovskite formation process ($PbI_2 + MAI \rightarrow MAPbI_3$), corresponds to the development of perovskite compound characterized by a higher thermodynamic stability. Consequently, adding starch into perovskite precursor solutions can produce perovskite films energetically more stable.

To go deeper into the crystallization behavior of the composite, we have performed time resolved GIWAXS during spin coating of perovskite precursors dissolved in DMSO at 6000

rpm and the results are shown in Figure 3. We have selected, among the analyzed samples by DSC, the one used in our previous works [20] (30MAPbI$_3$-15S) for photovoltaic devices, and the one with the lowest starch content (30MAPbI$_3$-5S). On the x-axis, we have time (s) and on the y-axis, we have q (nm^{-1}), and the z-scale is representative of intensity. Experiments were performed with the exposure time of 0.2 s and incident angle was kept fixed at 0.5°. In all cases we observe the presence of a wet, colloidal precursor phase as indicated by the formation of a broad scattering halo at low q values. In the case of pristine solution (a), not containing starch, solidification starts at around 50 s. As the film dries, we observe highly ordered precursor solvates at 4.36, 4.8 and 6.2 nm^{-1} which is the evidence of formation of solute solvent complex [24,25]. When the 5 wt% of starch was added in a precursor solution (b), it promotes gel phase existence for longer time, delaying the formation of ordered solvates up to 80 s, leading thus to delayed crystallization process. Similarly, when the concentration of starch was increased further up to 15 wt% (c), the delay time in formation of these ordered phase is increased to around 160 s. In figure 3(d), we have compared the peaks related to the solvate formed during the spin coating. It is evident that the highest intensity is recorded for the film containing the highest starch concentration (30MAPbI$_3$-15S) which is followed by the lowest and pristine respectively of the peak at 4.3 nm^{-1}. We have shown the evolution of the 4.3 nm^{-1} peak with time in figure 3(e). It is observable that in the case of pristine, the peak evolves first and stabilizes and it is followed by 30MAPbI$_3$-5S and 30MAPbI$_3$-15S respectively. We have performed time resolved GIWAXS during spin coating of pure starch solution, as blanc, and found no ordered structure (d). These experiments indicate that the starch plays an important role in delaying nucleation and assembly process, further corroborating the results form DSC experiments.

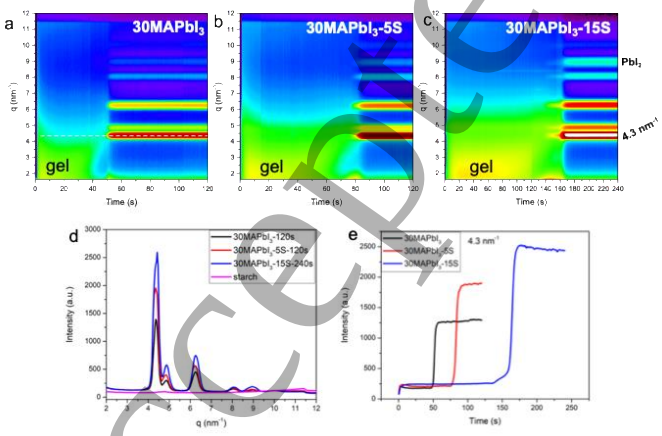

Figure 3. 2D intensity maps during film formation from a) the pristine prevoskite precursor solution, and solutions comprising b) 5 wt% and c) 15 wt% starch, respectively. d) Individual q-plots. e) Evolution of the 4.3 nm-1 peak with time.

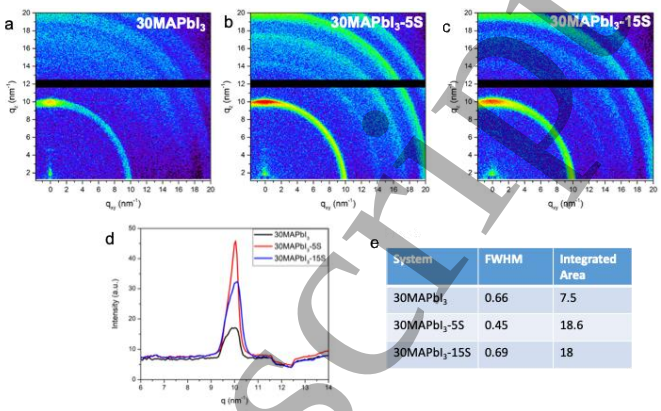

System	FWHM	Integrated Area
30MAPbI$_3$	0.66	7.5
30MAPbI$_3$-5S	0.45	18.6
30MAPbI$_3$-15S	0.69	18

Figure 4. GIWAXS patterns of the annealed films from a) the pristine prevoskite precursor solution, and solutions comprising b) 5 wt% and c) 15 wt% starch, respectively.

In Figure 4 we show the GIWAXS patterns of the annealed films from the three samples under examination. Thermal annealing process has eliminated all the precursor solvates by conversion to perovskite, which is the only signature present in the GIWAXS patterns at q = 10 nm^{-1}. We have compared the peaks at q = 10 nm^{-1} for each sample in figure 4(d/e). Perovskite peak from the pristine sample is lowest in intensity amongst all with FWHM of 0.66 nm^{-1}. The same peak from 30MAPbI3-5S shows a significant increase in intensity and a concomitant decrease in FWHM of 0.45 nm^{-1}. Peak from 30MAPbI3-15S shows a lower intensity than 30MAPbI3-5S (although higher than the pristine sample) and higher FWHM of 0.69 nm^{-1} similar to the pristine sample. This suggests that with the small amount of addition of starch induces better crystallinity (30MAPbI3-5S), but as the starch amount exceeds the 5 wt% concentration, we observe increase in FWHM and decrease in intensity, although higher than the pristine sample.

The better crystallinity for the starch-containing samples (Fig. 4) and the thermodynamically more stable material obtained maybe a direct consequence of the increased longevity of the wet precursors phase with the addition of starch (Fig. 3) and the widening of the crystallization window also determined by DSC measurements. Those changes in the formation process of perovskite in the presence of starch are likely responsible of improved stability to moisture and good transport properties of the perovskite film.

Conclusions

Our study reveals that the disordered sol–gel state, lasting several second in the pristine perovskite solution, can be stabilized and its longevity extended to minutes if starch additive is present. This has been confirmed both by differential scanning calorimetry measurements, that allowed to study the crystallization temperature and enthalpy of our system, and by time resolved GIWAXS performed during spin-coating. The importance of the precursor solvate phase longevity is determined by superior composite perovskite:starch film final microstructure. This likely translate into a drastically more robust active media, towards exposure to moisture. Furthermore, this deposition time broadening of perovskites facilitates their reproducible fabrication. The combined characterization presented here can be extended to various polymers/additives and different perovskites compositions as a prescreening on perovskite material formation, allowing to predict material prerogative towards more stable and efficient optoelectronic devices.

Acknowledgements

This research was funded by PON Project "Tecnologia per celle solari bifacciali ad alta Efficienza a 4 terminali per utility scale" (BEST-4U), of the Italian Ministry MIUR (CUP B88D19000160005)". The authors thank Giulio Zecca for carrying out the DSC measurements.

References

[1] Gong J, Flatken M, Abate A, Correa-Baena J-P, Mora-Seró I, Saliba M and Zhou Y 2019 The Bloom of Perovskite Optoelectronics: Fundamental Science Matters *ACS Energy Lett.* **4** 861–5

[2] Stranks S D and Snaith H J 2015 Metal-halide perovskites for photovoltaic and light-emitting devices *Nat. Nanotechnol.* **10** 391–402

[3] Li C, Wang A, Xie L, Deng X, Liao K, Yang J, Li T and Hao F 2019 Emerging alkali metal ion (Li+, Na+, K+ and Rb+) doped perovskite films for efficient solar cells: recent advances and prospects *J. Mater. Chem. A* **7** 24150–63

[4] Chen Y, Zhang L, Zhang Y, Gao H and Yan H 2018 Large-area perovskite solar cells–a review of recent progress and issues *RSC Adv.* **8** 10489–508

[5] Giuri A, Yuan Z, Miao Y, Wang J, Gao F, Sestu N, Saba M, Bongiovanni G, Colella S and Corcione C E 2018 Ultra-Bright Near-Infrared Perovskite Light-Emitting Diodes with Reduced Efficiency Roll-off *Sci. Rep.* **8** 15496

[6] Colella S, Mazzeo M, Rizzo A, Gigli G and Listorti A 2016 The Bright Side of Perovskites *J. Phys. Chem. Lett.* **7** 4322–4334

[7] Li Z, Klein T R, Kim D H, Yang M, Berry J J, van Hest M F A M and Zhu K 2018 Scalable fabrication of perovskite solar cells *Nat. Rev. Mater.* **3** 18017

[8] Li T, Pan Y, Wang Z, Xia Y, Chen Y and Huang W 2017 Additive engineering for highly efficient organic–inorganic halide perovskite solar cells: recent advances and perspectives *J. Mater. Chem. A* **5** 12602–52

[9] Masi S, Rizzo A, Aiello F, Balzano F, Uccello-Barretta G, Listorti A, Gigli G and Colella S 2015 Multiscale morphology design of hybrid halide perovskites through a polymeric template *Nanoscale* **7** 18956–63

[10] Masi S, Rizzo A, Munir R, Listorti A, Giuri A, Esposito Corcione C, Treat N D, Gigli G, Amassian A, Stingelin N and Colella S 2017 Organic Gelators as Growth Control Agents for Stable and Reproducible Hybrid Perovskite-Based Solar Cells *Adv. Energy Mater.* **7**

[11] Masi S, Aiello F, Listorti A, Balzano F, Altamura D, Giannini C, Caliandro R, Uccello-Barretta G, Rizzo A and Colella S 2018 Connecting the solution chemistry of PbI 2 and MAI: a cyclodextrin-based supramolecular approach to the formation of hybrid halide perovskites *Chem. Sci.* **9** 3200–8

[12] Dualeh A, Tétreault N, Moehl T, Gao P, Nazeeruddin M K and Grätzel M 2014 Effect of annealing temperature on film morphology of organic–inorganic hybrid pervoskite solid-state solar cells *Adv. Funct. Mater.* **24** 3250–8

[13] Nie W, Tsai H, Asadpour R, Blancon J-C, Neukirch A J, Gupta G, Crochet J J, Chhowalla M, Tretiak S and Alam M A 2015 High-efficiency solution-processed perovskite solar cells with millimeter-scale grains *Science (80-.).* **347** 522–5

[14] Huang Z, Hu X, Liu C, Tan L and Chen Y 2017 Nucleation and Crystallization Control via Polyurethane to Enhance the Bendability of Perovskite Solar Cells with Excellent Device Performance *Adv. Funct. Mater.* **27** 1703061

[15] Salado M, Jodlowski A D, Roldan-Carmona C, de Miguel G, Kazim S, Nazeeruddin M K and Ahmad S 2018 Surface passivation of perovskite layers using heterocyclic halides: Improved photovoltaic properties and intrinsic stability *Nano Energy* **50** 220–8

[16] Zhou X, Zhang Y, Kong W, Hu M, Zhang L, Liu C, Li X, Pan C, Yu G, Cheng C and Xu B 2018 Crystallization manipulation and morphology evolution for highly efficient perovskite solar cell fabrication via hydration water induced intermediate phase formation under heat assisted spin-coating *J. Mater. Chem. A* **6** 3012–21

[17] Masi S, Sestu N, Valenzano V, Higashino T, Imahori H, Saba M, Bongiovanni G, Armenise V, Milella A and Gigli G 2020 Simple Processing Additive-Driven 20% Efficiency for Inverted Planar Heterojunction Perovskite Solar Cells *ACS Appl. Mater. Interfaces* **12** 18431–6

[18] Masi S, Colella S, Listorti A, Roiati V, Liscio A, Palermo V, Rizzo A and Gigli G 2015 Growing perovskite into polymers for easy-processable optoelectronic devices *Sci. Rep.* **5** 1–7

[19] Giuri A, Saleh E, Listorti A, Colella S, Rizzo A, Tuck C and Esposito Corcione C 2019 Rheological tunability of perovskite precursor solutions: From spin coating to inkjet printing process *Nanomaterials* **9** 582

[20] Giuri A, Masi S, Listorti A, Gigli G, Colella S, Corcione C E and Rizzo A 2018 Polymeric rheology modifier allows single-step coating of perovskite ink for highly efficient and stable solar cells *Nano Energy* **54** 400–8

[21] Richter L J, DeLongchamp D M and Amassian A 2017 Morphology development in solution-processed functional organic blend films: an in situ viewpoint *Chem. Rev.* **117** 6332–66

[22] Schlipf J and Müller-Buschbaum P 2017 Structure of Organometal Halide Perovskite Films as Determined with Grazing-Incidence X-Ray Scattering Methods *Adv. Energy Mater.* **7** 1700131

[23] Munir R, Sheikh A D, Abdelsamie M, Hu H, Yu L, Zhao K, Kim T, Tall O El, Li R and Smilgies D 2017 Hybrid Perovskite Thin-Film Photovoltaics: In Situ Diagnostics and Importance of the Precursor Solvate Phases *Adv. Mater.* **29** 1604113

[24] Lee S, Tang M-C, Munir R, Barrit D, Kim Y-J, Kang R, Yun J-M, Smilgies D-M, Amassian A and Kim D-Y 2020 In situ study of the film formation mechanism of organic–inorganic hybrid perovskite solar cells: controlling the solvate phase using an additive system *J. Mater. Chem. A* **8** 7695–703

[25] Li J, Munir R, Fan Y, Niu T, Liu Y, Zhong Y, Yang Z, Tian Y, Liu B and Sun J 2018 Phase transition control for high-performance blade-coated perovskite solar cells *Joule* **2** 1313–30